Electron Raman scattering in $Hg_{1-x}Cd_xTe$ with inverted band structure

S. I. ZEYNALOVA[1,2,*], T. H. ISMAYILOV[2]
[1]*Institute of Physics of the Ministry of Science and Education of the Republic of Azerbaijan, Baku, Azerbaijan*
[2]*Baku State University, Baku, Azerbaijan*

The interband electronic Raman scattering (IERS) for $Hg_{1-x}Cd_xTe$ with the inverted band structure within the framework of the two-band Kane model is considered. The calculations of the differential effective cross section (DECS) are made. DECS for XX polarizations of incident and scattered radiation are calculated and its dependences on the frequency shift and "band-gap" ε_g is obtained. A number of general features of the scattering process and the resulting Raman spectrum are examined. The non-resonant and resonant cases are considered. In both cases, the dependences of DECS on the frequency shift are plotted for various values of the band gap.

(Received February 26, 2024; accepted July 30, 2024)

Keywords: Electronic Raman scattering, Kane model, Zero-gap semiconductor $Hg_{1-x}Cd_xTe$

1. Introduction

Solid solutions $Hg_{1-x}Cd_xTe$ have proven their advantages in practice, and there are now quite a lot of areas where they are used. Thermal imaging equipment based on the use of photodetectors in the infrared range for wavelengths of 1–30 μm is used in various areas. HgCdTe is the only common material that can detect infrared radiation in both of the accessible atmospheric windows. These are from 3 to 5 μm (the mid-wave infrared window, MWIR) and from 10 to 12 μm (the long-wave window, LWIR). HgCdTe can also detect in the shortwave infrared (SWIR) atmospheric windows of 2.2 to 2.4 μm and 1.5 to 1.8 μm. It has many more competitors today than ever before. These include silicone Schottky diodes, SiGe heterojunctions, AlGaAs multi-quantum well structures, superlattices based on strained GaInSb layers, high-temperature superconductors, and two types of thermal detectors: pyroelectric detectors and silicone bolometers. However, none of the above can compete with HgCdTe in fundamental properties. They may be more advanced, but will never provide better performance or, with the exception of thermal detectors, operate at higher or even comparable temperatures. The main advantages of HgCdTe are a direct band gap, the ability to obtain both low and high concentrations of charge carriers, high electron mobility and low dielectric constant. An extremely small change in the crystal lattice period with a change in composition makes it possible to grow high-quality multilayer structures and structures with a stepped bandgap [1-4].

The band structure of $Hg_{1-x}Cd_xTe$, depending on the composition (x), can be both normal, i.e. semiconductor (x>0.15; InSb type), and inverse, i.e. semi-metallic (x< 0.16; type of α–Sn, HgTe).

The energy distance between the bottom of the conduction band and the top of the valence band can vary from (-0.3) eV (x=0, HgTe) to +1.6 eV (x=1, CdTe). With an increase in the width ε_g starting from (-0.3 eV) at $\varepsilon_g = 0$, the band structure changes from inverse to normal band structure, i.e., $Hg_{1-x}Cd_xTe$ covers a fairly wide range of the spectrum, which includes the entire infrared region, as well as a part of the near-ultraviolet region [1,2].

Electronic Raman scattering is one of the powerful method for studying the electronic structure of semiconductors [5-8] and nanostructures based on them [9-12]. In this paper we consider the possible interband electronic Raman scattering (IERS) for $Hg_{1-x}Cd_xTe$ with the inverted band structure within the framework of the two-band Kane model.

2. General formula

The formula for differential effective cross section (DECS) of electron Raman scattering (ERS) is given in many works [5-8]. Here we will use the formula given by Y. Yafet [7].

$$\frac{d^2S}{d\Omega d\omega} = r_0^2 \frac{\omega_1}{\omega_0} \sum_{i,f} \left|A_{fi}\right|^2 \hbar\delta(\hbar\omega - E_f + E_i) \quad (1)$$

here Ω is solid angle, ω_0 and ω_1 are the incident and scattered light, correspondingly, $\omega = \omega_0 - \omega_1$ is the frequency shift, $r_0 = e^2/m_0c^2$ is the classical radius of the electron, and

$$A_{fi} = \frac{1}{m_0} \sum_r \left[\frac{(\vec{e}_1{}^* \vec{p})_{fr} (\vec{e}_0 \vec{p})_{ri}}{\varepsilon_i + \hbar\omega_0 - \varepsilon_r} + \frac{(\vec{e}_0 \vec{p})_{fr} (\vec{e}_1{}^* \vec{p})_{ri}}{\varepsilon_i - \hbar\omega_1 - \varepsilon_r} \right] \quad (2)$$

is a dimensionless composite matrix element, where i, f, r indicate the initial, final and intermediate state, correspondingly, $\varepsilon_i, \varepsilon_f, \varepsilon_r$ are the corresponding energies and $\vec{e}_0, \vec{e}_1$ are the polarizations of the incident and scattered radiation, respectively.

In (1), the summation covers all filled initial and empty final states. In this paper we consider the interband electronic Raman scattering (IERS) for $Hg_{1-x}Cd_xTe$ with the inverted band structure within the framework of the two-band Kane model[13].

The determination of the Raman cross section is reduced, according to (2) to the calculation of the composite matrix element A_{fi}, which, as is obvious, requires knowledge of the spectrum and wave functions of one-electron states.

3. Spectrum and wave functions

Fig. 1 shows the inverted band structure near the center of the Brillouin zone $\vec{k} = 0$ in two-band Kane model and the possible interband electronic Raman scattering[10].

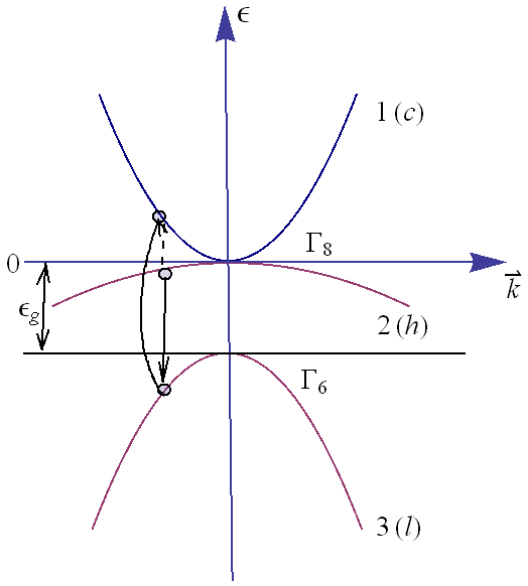

Fig. 1. Inverted band structure of $Hg_{1-x}Cd_xTe$ (x< 0.15) *near the center of the Brillouin zone* $\vec{k} = 0$ *in two-band Kane model and the possible interband electronic Raman scattering (color online)*

From the solution of the Schrödinger equation for the two-band Kane model (Fig. 1) we obtain the wave functions and electron spectrum of the corresponding bands:

$$\psi_{1k\uparrow}(r) = \left[\frac{\varepsilon_1(\vec{k}) + \varepsilon_g}{2\varepsilon_1(\vec{k}) + \varepsilon_g}\right]^{\frac{1}{2}} \times$$

$$\times \left\{ \frac{\varepsilon_1(\vec{k})u_1}{\sqrt{\frac{2}{3}}Pk} + \sqrt{\frac{3}{2}}\frac{k_+}{k}u_3 + \frac{k_z}{k}u_4 - \frac{1}{2}\frac{k_-}{k}u_5 \right\} e^{i\vec{k}\cdot\vec{r}}$$

$$\psi_{2k\uparrow}(r) = \left\{ -\frac{k_z}{k}\frac{k_+^2}{k_\perp^2}u_3 + \sqrt{\frac{3}{2}}\frac{k_+}{k}u_4 + -\frac{1}{2}\frac{k_-}{k}u_6 \right\} e^{i\vec{k}\cdot\vec{r}}$$

$$\psi_{3k\uparrow}(r) = \left[\frac{\varepsilon_3(\vec{k}) + \varepsilon_g}{2\varepsilon_1(\vec{k}) + \varepsilon_g}\right]^{\frac{1}{2}} \times$$

$$\times \left\{ \frac{\varepsilon_3(\vec{k})u_1}{\sqrt{\frac{2}{3}}Pk} + \sqrt{\frac{3}{2}}\frac{k_+}{k}u_3 + \frac{k_z}{k}u_4 - \frac{1}{2}\frac{k_-}{k}u_5 \right\} e^{i\vec{k}\cdot\vec{r}}$$

$$\psi_{nk\downarrow}(\vec{r}) = \hat{R}\psi_{nk\uparrow}(\vec{r}) \quad \hat{R} = \hat{K}\hat{I} \tag{3}$$

Here $\hat{K}$ is the time-reversal operator and $\hat{I}$ is the space-inversion operator, u_1 to u_6 are the Bloch amplitudes,

$$\mathbf{k}_\pm = k_x \pm ik_y, \quad k_\perp^2 = k_x^2 + k_y^2$$

$$u_1 = iS\downarrow\rangle; \qquad u_2 = iS\uparrow\rangle,$$

$$u_3 = \frac{1}{\sqrt{2}}|(X - iY)\downarrow\rangle; \qquad u_4 = \sqrt{\frac{2}{3}}|Z\downarrow\rangle + \frac{1}{\sqrt{6}}|(X - iY)\uparrow\rangle,$$

$$u_5 = \sqrt{\frac{2}{3}}Z\uparrow\rangle - \frac{1}{\sqrt{6}}|(X + iY)\downarrow\rangle; \tag{4}$$

$$\varepsilon_1(\vec{k})\left(\varepsilon_3(\vec{k}) + \varepsilon_g\right) = \frac{2}{3}P^2k^2$$

$$P = -\frac{\hbar}{m_0}\langle S|\nabla_z|Z\rangle \qquad \varepsilon_2(\vec{k}) = -\frac{\hbar^2k^2}{2m_h}$$

$$\varepsilon_3(\vec{k}) = -\varepsilon_1(\vec{k}) - \varepsilon_g$$

4. Calculation of the differential effective cross section

Since direct optical transitions of the type (l)-(c), (h)-(l) are allowed by the symmetry of the crystal, the IERS process takes place, which is shown in Fig. 2.

An incident photon with a frequency ω_0 excites an electron from the zone of light holes (l) to the conduction bands (c). In the second act, an electron from the zone of heavy holes "rolls" into the formed hole in the zone (l) and emits a photon with a frequencyω_1. The frequency shift $\omega = \omega_0 - \omega_1$ is equal to the excitation energy of the electron-hole pair formed in the scattering process. At T=0 zone (l) and (h) are completely filled, and the area (c) is empty. The states of electrons in the zones c, h, l will be denoted, respectively $|c\vec{k}\sigma_1>$, $|h\vec{k}\sigma_2>$, $|l\vec{k}\sigma_3>$.

In formula (1), we pass from the sum over $\vec{k}$ to integration.

$$\frac{d^2s}{d\Omega d\omega} = r_0^2 \frac{\hbar}{(2\pi)^3}\frac{\omega_1}{\omega_0}\sum_{\sigma_1\sigma_2}\int \frac{k^2 dk}{d\varepsilon_1}|A_{ch}|^2 \times \times \delta(\hbar\omega + \varepsilon_2 + \varepsilon_1)d\varepsilon_1 d\Omega(\vec{k}). \quad (5)$$

Let us express ε_2 by ε_1.Then we obtain

$$\varepsilon_2 = -\frac{3\hbar^2}{4m_h P^2}(\varepsilon_1 + \varepsilon_g)\varepsilon_1 = -\frac{\varepsilon_1(\varepsilon_1+\varepsilon_g)}{\varepsilon_0}, \quad \varepsilon_0 = \frac{4m_h P^2}{3\hbar^2} \quad (6)$$

Here we introduce the parameter ε_0, the characteristic energy, which is practically a constant value for the materials we are considering. At $m_h = 0.4m_0$, $P = 8\cdot 10^{-8}$eV·cm; $\varepsilon_0 \approx 4.48$ eV. Then we find that,

$$\rho(\varepsilon_1) = \frac{k^2 dk}{d\varepsilon_1} = \frac{3\sqrt{3}}{4\sqrt{2}P^3}(2\varepsilon_1 + \varepsilon_g)\varepsilon_1{}^{1/2}(\varepsilon_1 + \varepsilon_g)^{1/2} \quad (7)$$

Integration in (5) is simply removed using the δ-function and

$$\frac{d^2S}{d\Omega d\omega} = r_0^2 \frac{\hbar}{(2\pi)^3}\frac{\omega_1}{\omega_0}\rho(\lambda)\sum_{\sigma_1\sigma_2}\int |A_{ch}|^2 \frac{1}{|\varphi'(\lambda)|}d\Omega(\vec{k}), \quad (8)$$

where λ- is the solution of the equation $\varphi(\varepsilon_1) = 0$, under δ-function

$$\lambda = \frac{(\varepsilon_0+\varepsilon_g)}{2}\left[\sqrt{1 + \frac{4\hbar\omega\varepsilon_0}{(\varepsilon_0+\varepsilon_g)^2}} - 1\right] \quad (9)$$

Since this is

$$|\varphi'(\lambda)| = 1 + \frac{\varepsilon_g}{\varepsilon_0}\left(1 + \frac{4\hbar\omega\varepsilon_0}{(\varepsilon_0+\varepsilon_g)^2}\right)^{1\backslash 2} \approx 1$$

we can write;

$$\frac{d^2S}{d\Omega d\omega} = r_0^2 \frac{\hbar\omega_1}{(2\pi)^3\omega_0}\rho(\lambda)\sum_{\sigma_1\sigma_2}\int |A_{ch}(\lambda)|^2 d\Omega(\vec{k}) \quad (10)$$

Here;

$$A_{ch}(\lambda) = \frac{1}{m_0 A(\lambda)}\cdot \sum_{\sigma_3}\langle c\vec{k}\sigma_1|P_I|l\vec{k}\sigma_3\rangle\langle l\vec{k}\sigma_3|P_S|h\vec{k}\sigma_2\rangle + \frac{1}{m_0 B(\lambda)}\cdot \sum_{\sigma_3}\langle c\vec{k}\sigma_1|P_S|l\vec{k}\sigma_3\rangle\langle l\vec{k}\sigma_3|P_I|\vec{h}k\sigma_2\rangle, \quad (11)$$

$$A(\lambda) = 2\lambda + \varepsilon_g - \hbar\omega_0,\ B(\lambda) = \lambda + \varepsilon_g + \hbar\omega_0 \quad (12)$$

P_I and P_S are the projections of the momentum operator on the polarization directions of the incident and scattered photons, respectively.

5. XX Scattering

Let us consider the case when the incident and scattered light are polarized along the X axis. Then formula (10) takes the form

$$\frac{d^2S_{xx}}{d\Omega d\omega} = \frac{r_0^2\hbar\omega_1}{(2\pi)^3\omega_0}\rho(\lambda)\left[\frac{1}{A(\lambda)} + \frac{1}{B(\lambda)}\right]^2\int d\Omega(\vec{k})\sum_{\sigma_1\sigma_2}\left|\frac{1}{m_0} \times \langle c\vec{k}\sigma_1|p_x|l\vec{k}\sigma_3\rangle\langle l\vec{k}\sigma_3|p_x|h\vec{k}\sigma_2\rangle^2\right| \quad (13)$$

Using the explicit form of the wave functions (3), we find that

$$\int d\Omega(\vec{k})\sum_{\sigma_1\sigma_2}\left|\frac{1}{m_0}\sum_{\sigma_3}\langle c\vec{k}\sigma_1|p_x|l\vec{k}\sigma_3\rangle\langle l\vec{k}\sigma_3|p_x|h\vec{k}\sigma_2\rangle^2\right| = = \frac{16\pi P^4}{45\hbar^4}\cdot\frac{\lambda+\varepsilon_g}{2\lambda+\varepsilon_g}\left(1 + \frac{\varepsilon_g^2}{(2\lambda+\varepsilon_g)^2}\right) \quad (14)$$

Substituting (14) into (13) we finally obtain

$$\frac{d^2S_{xx}}{d\Omega d\omega} = r_0^2\cdot\frac{m_0^2 P}{10\sqrt{6}\pi^2\hbar^3}\frac{\omega_0-\omega}{\omega_0}\cdot\Phi(\lambda) \quad (15)$$

where

$$\Phi(\lambda) = \lambda^{\frac{1}{2}}(\lambda+\varepsilon_g)^{\frac{3}{2}}\cdot\left[\frac{1}{A(\lambda)} + \frac{1}{B(\lambda)}\right]^2\left(1 + \frac{\varepsilon_g^2}{(2\lambda+\varepsilon_g)^2}\right) \quad (16)$$

is a dimensionless function.

It can be seen from formulas (15) and (16) that for $\varepsilon_g \to \infty$ (parabolic limit) we obtain the corresponding formulas of the work [14].

6. The discussion of the results

It is seen from the expression (15) for XX scattering that the DECS spectrum extends from $\omega = 0$ to $\omega = \omega_0$. Let $\hbar\omega_0 < \varepsilon_g$. In this case, at low frequencies $\omega << \omega_0$ DES continues to grow, then reaching the maximum, decreases to zero.

But if $\hbar\omega_0 > \varepsilon_g$, resonance occurs, when $A(\lambda) = 0$, that is;

$$\hbar\omega = \frac{\hbar\omega_0 - \varepsilon_g}{2}\left(1 + \frac{\hbar\omega_0 + \varepsilon_g}{2\varepsilon_0}\right) \qquad (17)$$

This resonance corresponds to real transitions between zones (l) and (c) caused by incident radiation and real transition between (l)-(c), (h) and (l) caused by scattered radiation. Knowing the values of ω_0, P and m_h from the position of the resonance peak, one can find the experimental value of ε_g.

It follows from expression (17) that taking into account the non-parabolicity leads to a shift of the resonant point to the right, by the value;

$$\Delta\hbar\omega = \frac{\hbar\omega_0 - \varepsilon_g}{2} \cdot \frac{\hbar\omega_0 + \varepsilon_g}{2\varepsilon_0} \qquad (18)$$

Fig. 2 shows the dependence of the DECS on the frequency shift for two values of ε_g ($\varepsilon_g = 0.3eV$ and 0.2eV). For $\hbar\omega_0$ is taken the value 0.117 eV (CO_2 laser line) and P = $8 \cdot 10^{-8}$ eV·cm. As can be seen from the figure 3, with a decrease of ε_g, the DECS maximum increases and when $\hbar\omega_0 < \varepsilon_g$ scattering is non-resonant. But when $\hbar\omega_0 > \varepsilon_g$ the scattering becomes resonant. It follows from Fig. 3 that with decreasing ε_g the resonant frequency shifts towards higher energies (to the short-wavelength region of the spectrum). In this case, the DECS of IERS are of great values, which indicates the possibility of obtaining a laser effect based on the IERS.

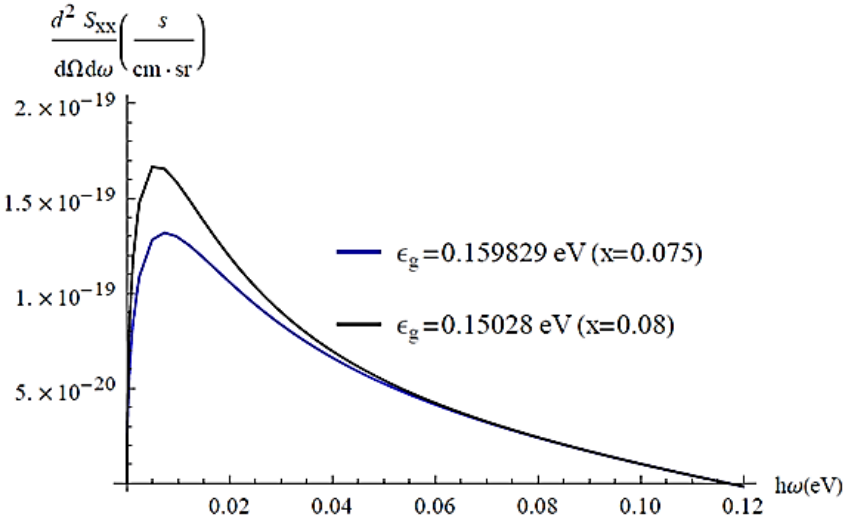

Fig. 2. Plot of DECS as a function of frequency shift of non-resonant ($\hbar\omega_0 < \varepsilon_g$) IERS for two values of ε_g (color online)

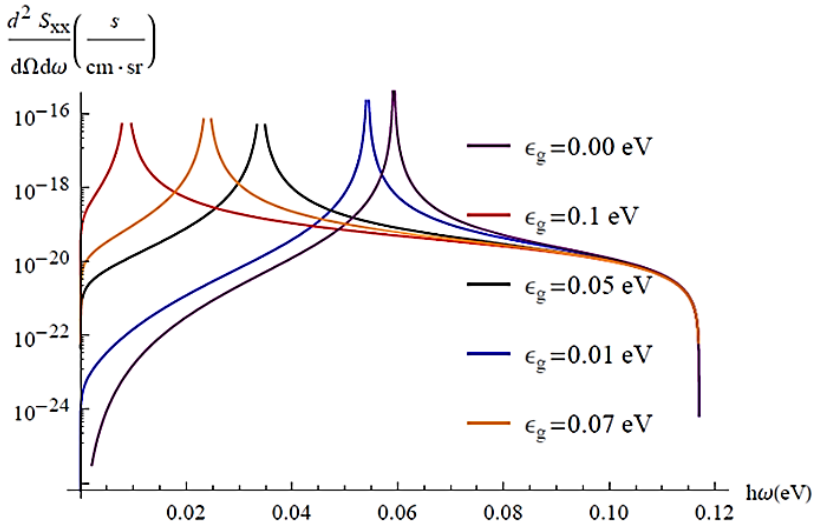

Fig. 3. LogPlot of DECS as a function of frequency shift of resonant ($\hbar\omega_0 > \varepsilon_g$) IERS for five values of ε_g (color online)

A qualitatively different situation occurs in the gapless state $\varepsilon_g = 0$. In this case, formula (15) takes the form

$$\frac{d^2S_{xx}}{d\Omega d\omega} = r_0^2 \frac{m_0^2 P}{10\sqrt{6}\pi^2\hbar^3}\frac{\omega_0-\omega}{\omega_0}\lambda^2 \cdot \left|\frac{1}{2\lambda-\hbar\omega_0}+\frac{1}{\lambda+\hbar\omega_0}\right|^2 \quad (19)$$

where

$$\lambda = \frac{\varepsilon_0}{2}\cdot\left[\sqrt{1+\frac{4\hbar\omega}{\varepsilon_0}}-1\right] \quad (20)$$

One can immediately note that in this case only resonant scattering takes place. At low frequencies, expanding expression (20) in a power series $\frac{\hbar\omega}{\varepsilon_0}$ and restricting ourselves to the first two terms, we get that $\lambda \approx \hbar\omega$. Then

$$\frac{d^2S_{xx}}{d\Omega d\omega} = r_0^2 \frac{9m_0^2 P}{40\sqrt{6}\pi^2\hbar^3}\left(\frac{\omega}{\omega_0}\right)^2 \cdot \left|\frac{1}{\frac{2\omega}{\omega_0}-1}+\frac{1}{\frac{\omega}{\omega_0}+1}\right|^2 \quad (21)$$

that is, in the gapless state at low frequencies, the cross section depends quadratically on ω. As ω increases, the cross section decreases, so does

$$\omega = \frac{\omega_0}{2}\cdot\left(1+\frac{\hbar\omega}{2\varepsilon_0}\right) \approx \frac{\omega_0}{2} \quad (22)$$

resonance occurs. With further growth due to the factor $\frac{\omega_0-\omega}{\omega_0}$ DECS tends to zero. Note that, according to the position of the resonant frequency as a function of ε_g, one can observe the semimetal-semiconductor transition in the experiment. As can be seen from expression (18), with a decrease of ε_g, the resonant point shifts to the right, and at $\varepsilon_g = 0$, the transition point of semimetal-semiconductor has the value (22).

It also follows from the above that it is possible to build a laser, in the absence of a magnetic field, operating in a resonant mode, the frequency of which can be controlled by smoothly changing the bandgap ε_g.

So far, our discussions have referred to intrinsic materials at temperature T=0K. If there will be impurities, then the presence of electrons in the conduction band leads to the fact that the final states up to the Fermi level will be blocked and will not participate in the IERS process. In other words, the presence of free electrons shifts the IERS threshold to the right (the Moss-Burstein effect). This threshold is determined by the expression

$$\lambda_{thres} = \varepsilon_F = -\frac{\varepsilon_g}{2}+\sqrt{\frac{\varepsilon_g^2}{4}+\frac{2}{3}P^2k_F^2}, \quad (23)$$

$$k_F = (3\pi^2 n)^{2/3};$$

where n is a conduction-electron concentration.

One of the fundamental problems in the observation of interband Raman scattering is its difference from ordinary luminescence. Since electron-hole pairs are formed in the Raman process, recombination of electrons and holes can occur with simultaneous emission of light. Electrons and holes have certain lifetimes during which they can partially or completely thermalize before recombination occurs. Therefore, a broad luminescent band can be expected. Raman scattering from luminescence in the experiment can be distinguished using resonant peaks (peak positions), observing their shifts depending on the frequency of the incident light and the width of the band gap ε_g.

The calculations above were carried out in the single-particle approximation, i.e. we did not take into account exciton effects. Accounting for exciton effects can lead to a significant modification of the scattering spectrum. Clearly pronounced peaks associated with exciton transitions can be observed in the experiment. It should be noted that taking into account the Coulomb interaction between an electron

and a hole produced in the process of scattering can also turn out to be important.

References

[1] Wen Lei, Lorenzo Faraone, Jarek Antoszewski, Applied Physics Reviews **2**(4),041303, 041303 (2015).
[2] Mercury Cadmium Telluride: Growth, Properties and Applications, John Wiley & Sons Ltd., Edited by Peter Capper and James Garland, (2011).
[3] A. Rogalski, Rep. Prog. Phys. **68**, 2267 (2005).
[4] Junhao Chu, Arden Sher, Physics and Properties of Narrow Gap Semiconductors, Springer Science: Business Media, LLS, (2008).
[5] R. J. Elliott, R. Loudon, Physics Letters **3**(4), 189 (1963).
[6] P. A. Wolff, Phys. Rev. Letters **16**, 225 (1966).
[7] Y. Yafet, Phys. Rev. **152**, 858 (1966).
[8] S. S. Jha, Nuovo Cimento B **LXIII** B (1), 331 (1969).
[9] Ri. Betancourt-Riera, Re. Betancourt-Riera, L. A. Ferrer-Moreno, A. D. Sañu-Ginarte, Physica B: Physics of Condensed Matter **563**, 93 (2019).
[10] Dennis Kudlacik, Victor F. Sapega, Dmitri R. Yakovlev, Ina V. Kalitukha, Elena V. Shornikova, Anna V. Rodina, Eugeniius L. Ivchenko, Grigorii S. Dimitriev, Michel Nasilowski, Benoit Dubertret, Manfred Bayer, Nano Letters **20**(1), 517 (2020).
[11] A. V. Rodina, E. L. Ivchenko, Phys. Rev. B **102**, 235432 (2020).
[12] Ri. Betancourt-Riera, Re. Betancourt-Riera, L. A. Ferrer-Moreno, J. M. Nieto Jalil, Physica B **600**, 412640 (2021).
[13] E. O. Kane, J. Phys. Chem. Solids **1**, 257 (1957).
[14] E. Burstein, D. L. Mills, R. F. Wallis, Phys. Rev. B **4**, 2429 (1971).

*Corresponding author: sebine-zeynalova@mail.ru